Pseudorapidity distributions of charged particles in p-$\bar{p}$ or p-p collisions at high energies and predictions at ultrahigh energies

Jian-Xin Sun,[1,2] Fu-Hu Liu,[1,*] Er-Qin Wang,[1] Yan Sun,[3] and Zhu Sun[3]

[1]*Institute of Theoretical Physics, Shanxi University, Taiyuan, Shanxi 030006, People's Republic of China*

[2]*School of Engineering, Shanxi Datong University, Datong, Shanxi 037003, People's Republic of China*

[3]*School of Physics and Electronic Science, Shanxi Datong University, Datong, Shanxi 037009, People's Republic of China*

(Received 7 June 2010; revised manuscript received 17 November 2010; published 31 January 2011)

Pseudorapidity distributions of charged particles produced in p-$\bar{p}$ or p-p collisions at different energies were reported by the UA5, UA1, P238, CDF, and ALICE collaborations. A multisource ideal gas model is used to fit the experimental data in this paper. According to the parameter values obtained from fitting the data, we find different linear relationships between different parameters and logarithmic center-of-mass energy. A prediction for the pseudorapidity distributions of charged particles produced in p-$\bar{p}$ or p-p collisions at the higher Large Hadron Collider energies is given.

DOI: 10.1103/PhysRevC.83.014001 PACS number(s): 24.10.Pa, 25.75.Dw

I. INTRODUCTION

The Relativistic Heavy Ion Collider (RHIC) in the United States and the Large Hadron Collider (LHC) in Switzerland have been built, respectively, to research the properties of produced matter in collisions. The LHC was originally designed to accelerate two protons up to total energy of 14 TeV [1–3]. In December 2009 the LHC achieved already 2.3 TeV, which broke the record of 1.8 TeV set by the Fermilab in United States. Such high-energy collisions offer us the opportunity to research the Higgs and dark matter [4–6], as well as the particle statistical behavior at ultrahigh energy. The multiplicity and pseudorapidity distributions of particles can be used to test different theoretical models and ideas [7]. High-energy nucleon-nucleon and nucleus-nucleus collisions are of great help in understanding the particle statistical behavior, production process, interaction mechanism, and related phenomenon in high-density and high-temperature states.

Several collaborations have researched p-$\bar{p}$ or p-p collisions over an energy range from 53 to 1800 GeV. They are the UA1 (p-$\bar{p}$ collisions at 540 GeV [8]), UA5 (p-$\bar{p}$ collisions at 53, 200, 546, and 900 GeV [9]), P238 (p-$\bar{p}$ collisions at 630 GeV [10]), CDF (p-$\bar{p}$ collisions at 630 and 1800 GeV [11]), and ALICE (p-p collisions at 900 GeV on the November 23, 2009, during the early running stage at the LHC [12]). The UA5 and ALICE, respectively, did research work on two different normalizations: nonsingle diffractive (NSD) and inelastic (INEL) p-$\bar{p}$ or p-p collisions at 900 GeV [9,12]. In fact, the NSD and INEL collisions have a constant normalization of the cross section [9,12]. Following our recent investigation [13] and analysis of the experimental data with the multisource ideal gas model [14–17], we find the deviation between the two normalizations being less than 6%.

The rapidity distribution $dN_{\rm ch}/dy$ and the pseudorapidity distribution $dN_{\rm ch}/d\eta$ of charged particles are very important quantities for the study of particle production mechanism in high-energy nucleon-nucleon and nucleus-nucleus collisions. Both $dN_{\rm ch}/dy$ and $dN_{\rm ch}/d\eta$ can be used to measure the temperature and density of the quark-gluon plasma (QGP) [18–20]. They reflect the most particle contribution in heavy-ion collisions and also demonstrate the effects of parton shadowing, particle rescattering, and final-state particle interactions. The study of $dN_{\rm ch}/dy$ and $dN_{\rm ch}/d\eta$ in p-$\bar{p}$ or p-p collisions provides baseline and reference for heavy-ion collisions. At ultrahigh energies hot dense matter might be also created in p-$\bar{p}$ or p-p collisions.

According to our recent investigation [13] finished in the framework of the multisource ideal gas model [14–17], the experimental data of particle pseudorapidity distributions in p-$\bar{p}$ or p-p collisions measured by the above five collaborations [8–12] are analyzed in this paper. We can give the variation law of different parameters from the investigation and predict the pseudorapidity distributions in p-$\bar{p}$ or p-p collisions at the higher LHC energies.

II. THE MODEL

The participant-spectator picture is a base of nucleon-nucleon and nucleus-nucleus collision theories and many other theoretical models, such as the LEXUS model [21], the nuclear fireball model [22,23], the QMD model [24–27], the Glauber model [28], the two-component model [29,30], the threshold model [31,32], the HSD model [33–35], the nuclear overlap model [36], the multisource ideal gas model [14–17], and so on. In the frameworks of multisource ideal gas model and nuclear geometry theory, each nucleus goes straight in collisions. The overlapping parts of the two nuclei are called the participants, which consist of many emission sources to produce particles. The residual parts of the two nuclei are called the spectators in which many emission sources are excited to emit nuclear fragments.

According to the multisource ideal gas model, a projectile cylinder and a target cylinder are produced when the projectile and target pass each other. Our analysis shows that the overlapping extent of the two cylinders decreases with

*fuhuliu@163.com; liufh@mail.sxu.cn

the increase of collision energy. In the ultrahigh-energy region, the distance between the two cylinders increases with the increase of collision energy. In the laboratory reference system, we assume that the projectile cylinder is in the positive rapidity direction and the target cylinder is in the negative one, with rapidity ranges $[y_{P\min}, y_{P\max}]$ and $[y_{T\min}, y_{T\max}]$, respectively. The projectile cylinder and target cylinder are assumed to be a series of isotropic emission sources with different rapidity shifts. On both sides of the two cylinders there are leading particles appearing as two isotropic emission sources with rapidity shifts y_P and y_T, respectively. It is expected that a thick double cylinder is formed in nucleus-nucleus collisions and a thin double cylinder is formed in nucleon-nucleon collisions.

According to the increasing direction of the rapidity coordinate scalar, we divide the collision system into four parts. They are the target leading particles (TL), target cylinder (TC), projectile cylinder (PC), and projectile leading particles (PL), respectively. To give a clear picture for understanding the definitions of variables and parts, different rapidity shifts for different parts in rapidity space are given in Fig. 1, where panels (a), (b), and (c) denote the situations of complete overlap, part overlap, and separation, respectively. It is expected that the colliding energy corresponding to the situation of separation is higher than that of overlap.

In the rest frame of a considered emission source with rapidity y_x in the TL, TC, PC, or PL, the pseudorapidity distribution of the produced particles is given by [37,38]

$$f(\eta, y_x) = \frac{1}{2\cosh^2(\eta - y_x)}. \tag{1}$$

If $y_x = y_P(y_T)$, the expression above can describe the pseudorapidity distribution of the projectile (target) leading particles. Mostly, y_x distributes equably in $[y_{P\min}, y_{P\max}]$ or

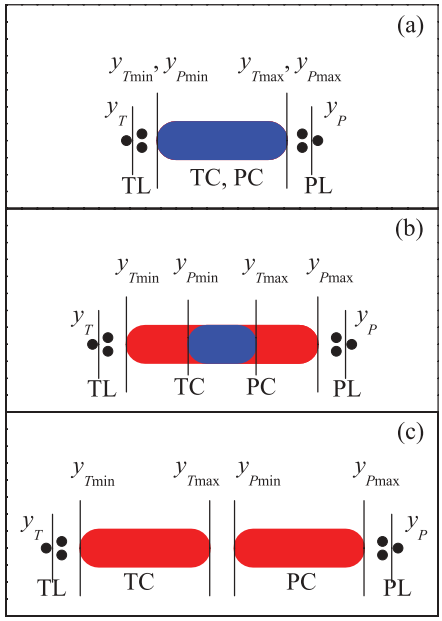

FIG. 1. (Color online) Relative positions among the TL, TC, PC, PL, and their rapidity shifts in rapidity space. Panels (a), (b), and (c) correspond to complete overlap, part overlap, and separation, respectively. The overlapping region in Fig. 1(b) is blue.

$[y_{T\min}, y_{T\max}]$. In the final state, the normalized pseudorapidity distribution can be expressed as [39]

$$\begin{aligned} f(\eta) = {} & \frac{k_T}{2\cosh^2(\eta - y_T)} + \frac{K_T}{2(y_{T\max} - y_{T\min})} \\ & \times \int_{y_{T\min}}^{y_{T\max}} \frac{dy_x}{\cosh^2(\eta - y_x)} + \frac{K_P}{2(y_{P\max} - y_{P\min})} \\ & \times \int_{y_{P\min}}^{y_{P\max}} \frac{dy_x}{\cosh^2(\eta - y_x)} + \frac{k_P}{2\cosh^2(\eta - y_P)}. \end{aligned} \tag{2}$$

In this expression, k_P, K_P, K_T, and k_T denote, respectively, the contributions of PL, PC, TC, and TL. Obviously, they are normalized to 1. For a symmetrical collision system, as given in our previous work [13], there are simple relationships among these parameters in Eq. (2). Generally, for a given normalized pseudorapidity distribution, some of k_P, K_P, K_T, k_T, $y_{P\min}$, $y_{P\max}$, $y_{T\min}$, $y_{T\max}$, y_P, and y_T are free parameters.

We use the Monte Carlo method to calculate the pseudorapidity distribution. According to the different contributions, the emission sources distribute randomly in the PC range $[y_{P\min}, y_{P\max}]$, TC range $[y_{T\min}, y_{T\max}]$, PL region, or TL region. Considering the particles emitted isotropically in the rest frame of the emission source, as in the Maxwell ideal gas model, the three components (P_x, P_y, P_z) of particle momentum obey Gaussian distributions with the same deviation σ. We have

$$\begin{aligned} P_x &= \sqrt{-2\ln R_1}\cos(2\pi R_2)\sigma, \\ P_y &= \sqrt{-2\ln R_3}\cos(2\pi R_4)\sigma, \\ P_z &= \sqrt{-2\ln R_5}\cos(2\pi R_6)\sigma. \end{aligned} \tag{3}$$

The emission angle and pseudorapidity are then given by

$$\theta = \arctan\frac{\sqrt{P_x^2 + P_y^2}}{P_z} \tag{4}$$

and

$$\eta = -\ln\tan\left(\frac{\theta}{2}\right), \tag{5}$$

respectively. In the final state, the pseudorapidity of particles produced in the two cylinders can be expressed as

$$\begin{aligned} \eta_{TC} &= (y_{T\max} - y_{T\min})R_7 + y_{T\min} + \eta, \\ \eta_{PC} &= (y_{P\max} - y_{P\min})R_8 + y_{P\min} + \eta. \end{aligned} \tag{6}$$

The pseudorapidity of leading particles can be expressed as

$$\begin{aligned} \eta_{TL} &= y_T + \eta, \\ \eta_{PL} &= y_P + \eta. \end{aligned} \tag{7}$$

In the expressions above, R_1, R_2, R_3, R_4, R_5, R_6, R_7, and R_8 are all random variables in interval [0,1], y and η are approximately equal to each other at high energy, and σ does not affect the calculated result owing to its disappearing in Eq. (4).

In the above discussions, there is an approximation of y and η, which is strongly dependent on the particle momentum. In Eq. (3), if we use a given σ for the particles produced in the cylinder regions (or a pion mass for those particles and a temperature parameter) and another σ for the leading

particles (or a proton mass and another temperature parameter) as well as the definition of y, then a non-negligible systematic uncertainty may be introduced. In our previous work [40], we distinguished y and η in Au-Au collisions at the RHIC energy by using a given σ. In fact, in the midrapidity region the difference between the two distributions is obvious, and in the forward region the difference between the values of y and η is obvious. We see that, considering the leading particles, another two parameters have been introduced in distinguishing y and η. In the present work, in the case of using an approximation of y and η, the main advantage is that a simple formula [Eq. (2)] could be obtained.

There is an assumption that the system of the model generated is isotropic and the momenta of particles are generated randomly. Especially, the three components are assumed to obey Gaussian distributions with the same width. It is expected that the present model cannot predict other quantities such as particle momentum distributions and correlations. If we assume that P_x and P_y obey Gaussian distributions with different widths and different nonzero average values, then a Rayleigh-like distribution and an anisotropic azimuthal distribution can be obtained to describe, respectively, the transverse momentum distribution and other quantities such as elliptic flow [41].

III. COMPARISON WITH EXPERIMENTAL DATA

Figure 2 shows the pseudorapidity distributions of charged particles produced in INEL p-$\bar{p}$ collisions at the center-of-mass energy $\sqrt{s} = 53$, 200, 546, and 900 GeV. The solid circles with the error bars represent the experimental data with the statistical errors measured by the UA5 Collaboration [9] and the open circles are symmetrical reflection at the mid-pseudorapidity $\eta = 0$. The curves are our calculated results with the multisource ideal gas model. For the solid curves shown in Figs. 2(a)–2(d), the corresponding parameter values obtained by fitting the experimental data are given in Table I with the values of χ^2 per degree of freedom (χ^2/dof). From these values we conclude that the $y_{P\max}$ ($-y_{T\min}$) and $y_{P\min}$ ($-y_{T\max}$) increase with the increase of collision energy. In other words, the length of the double cylinder and the distance between the two cylinders increase with the increase of collision energy. The other parameters are likely stable to be constant values, which means that the leading particle contribution to pseudorapidity distribution is nearly an invariable probability. From the figure we know that by using three rapidity shifts (such as $y_{P\min}$, $y_{P\max}$, and y_P) and one contribution (such as K_P or k_P) as free parameters, the multisource ideal gas model describes the pseudorapidity distributions of charged particles produced in INEL p-$\bar{p}$ collisions over an energy range from 53 to 900 GeV. We notice that the considered energy range covers the RHIC energies. Especially, the 200 GeV equals exactly one of the RHIC energies at which the data of p-p collisions is available and comparable.

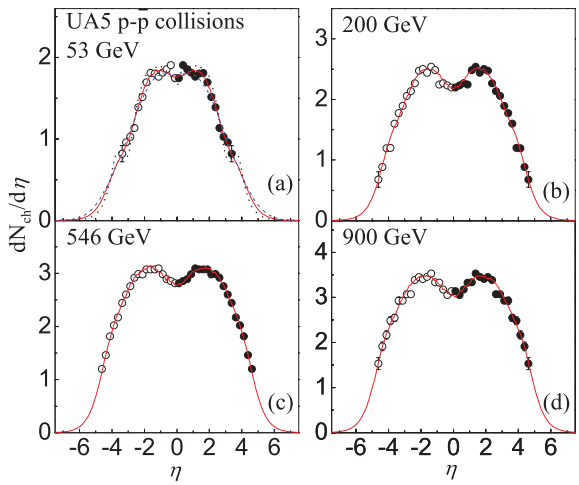

FIG. 2. (Color online) The pseudorapidity distributions of charged particles produced in INEL p-$\bar{p}$ collisions at $\sqrt{s} = 53$, 200, 546, and 900 GeV. The solid circles represent the measured data with the statistical errors of the UA5 Collaboration [9] and the open circles are symmetrical reflection at the mid-pseudorapidity $\eta = 0$. The curves are our calculated results with the multisource ideal gas model.

To study the change trends of pseudorapidity distribution when applying different distributions for the momentum components, we recalculate the result in Fig. 2(a) by different widths for P_x, P_y, and P_z distributions. The dotted curve corresponds to the result of the P_x distribution width being two times the width of P_y (and P_z) distribution, and the dashed curve corresponds to the result of the P_x distribution width being half of the width of P_y (and P_z) distribution. The corresponding values of χ^2/dof are 0.890 and 0.300, respectively. We see a small effect of different distributions. In fact, the main effect on the pseudorapidity distribution is produced by the length of the double cylinder, the distance between the two cylinders, and the contributions of leading particles.

The pseudorapidity distribution of charged particles produced in INEL p-$\bar{p}$ collisions measured by the UA1 Collaboration at $\sqrt{s} = 540$ GeV [8] is presented in Fig. 3. The symbols and curve have the same meanings as those in Fig. 2. By fitting

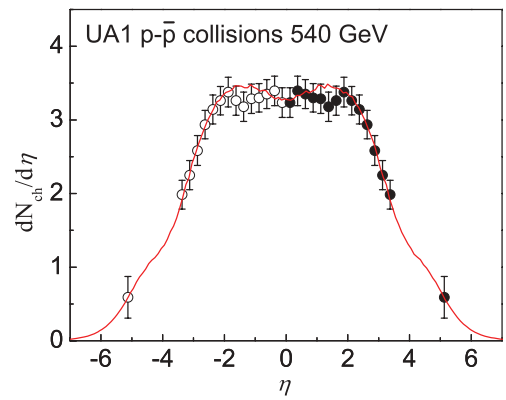

FIG. 3. (Color online) The pseudorapidity distribution of charged particles produced in INEL p-$\bar{p}$ collisions at $\sqrt{s} = 540$ GeV. The symbols and curve have the same meanings as those in Fig. 2, but the experimental data with the systematic errors are taken from the UA1 Collaboration [8].

TABLE I. Parameter values corresponding to the solid curves in Figs. 2–6.

Figure	Energy (GeV)	Collisions	$y_{P\max} = -y_{T\min}$	$y_{P\min} = -y_{T\max}$	$y_P = -y_T$	$K_P = K_T$	$k_P = k_T$	N_c	χ^2/dof
2(a)	53	p-$\bar{p}$	2.700 ± 0.100	0.080 ± 0.009	3.950 ± 0.050	0.415 ± 0.003	0.085 ± 0.003	7.200 ± 0.450	0.174
2(b)	200	p-$\bar{p}$	3.150 ± 0.080	0.120 ± 0.005	3.900 ± 0.030	0.410 ± 0.002	0.090 ± 0.002	17.500 ± 0.750	0.142
2(c)	546	p-$\bar{p}$	3.470 ± 0.050	0.148 ± 0.003	4.100 ± 0.020	0.415 ± 0.001	0.085 ± 0.001	25.800 ± 0.800	0.048
2(d)	900	p-$\bar{p}$	3.600 ± 0.060	0.170 ± 0.005	4.250 ± 0.030	0.410 ± 0.002	0.090 ± 0.002	29.800 ± 0.900	0.082
3	540	p-$\bar{p}$	3.400 ± 0.090	0.140 ± 0.005	4.500 ± 0.100	0.415 ± 0.005	0.085 ± 0.005	26.000 ± 0.850	0.120
4	630	p-$\bar{p}$	3.650 ± 0.080	0.150 ± 0.005	4.620 ± 0.050	0.415 ± 0.002	0.085 ± 0.002	28.100 ± 0.850	0.017
5(a)	630	p-$\bar{p}$	3.470 ± 0.050	0.162 ± 0.003	4.100 ± 0.050	0.410 ± 0.003	0.090 ± 0.003	28.500 ± 0.900	0.331
5(b)	1800	p-$\bar{p}$	3.850 ± 0.009	0.200 ± 0.002	4.000 ± 0.050	0.410 ± 0.002	0.090 ± 0.002	37.500 ± 0.950	0.105
6(a)	900	p-$\bar{p}$	3.550 ± 0.050	0.170 ± 0.002	—	0.500 ± 0.000	—	31.520 ± 0.950	0.093
6(b)	900	p-p	3.550 ± 0.050	0.170 ± 0.003	—	0.500 ± 0.000	—	29.900 ± 0.900	0.280

the experimental data, the obtained parameter values are given in Table I with the value of χ^2/dof. Although the collision energy for Fig. 3 is only 6 GeV, less than that for Fig. 2(c), the difference between the two figures seems to be existent. However, the UA1's research proves that the two experimental results are consistent within the error range [8]. We see that the multisource ideal gas model with four free parameters describes the pseudorapidity distribution of charged particles produced in INEL p-$\bar{p}$ collisions at 540 GeV, which is higher than the RHIC energies.

Figure 4 gives the pseudorapidity distribution of charged particles produced in INEL p-$\bar{p}$ collisions measured by the P238 Collaboration at $\sqrt{s} = 630$ GeV with $|\eta|$ ranging from 1.5 to 5.5 [10]. The symbols and curve represent the same meanings as those in Fig. 2. By fitting the experimental data, the obtained parameter values are given in Table I with the value of χ^2/dof. From the figure we know that the multisource ideal gas model with four free parameters describes the pseudorapidity distribution of charged particles produced in INEL p-$\bar{p}$ collisions at 630 GeV.

The pseudorapidity distributions of charged particles produced in INEL p-$\bar{p}$ collisions measured by the CDF Collaboration at $\sqrt{s} = 630$ and 1800 GeV with $|\eta|$ ranging from 0 to 3.5 [11] are shown in Fig. 5. The symbols and curves represent the same meanings as those in Fig. 2. By fitting the experimental data in Figs. 5(a) and 5(b), the obtained parameter values are given in Table I. From the figure we know that the multisource ideal gas model with four free parameters describes the pseudorapidity distributions of charged particles produced in INEL p-$\bar{p}$ collisions at 630 and 1800 GeV.

For the interactions NSD at $\sqrt{s} = 900$ GeV, the pseudorapidity distributions of charged particles measured by the UA5 Collaboration in p-$\bar{p}$ collisions with $|\eta| = 0$–2, and by the ALICE Collaboration in p-p collisions with $|\eta| = 0$-1.6 [12], are shown in Fig. 6. The symbols and curves represent the same meanings as those in Fig. 2. For the two curves in Figs. 6(a) and 6(b), the corresponding parameter values are given in Table I. In the calculation, the rapidity shift of leading particles is not available owing to their zero contribution in the narrow distribution. We see that the parameter values of the two interactions are almost the same. The difference for the two interactions is mainly in the normalization coefficients. From the figure we know that the multisource ideal gas model

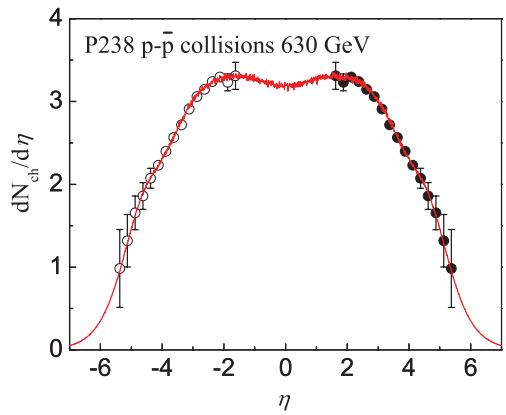

FIG. 4. (Color online) The pseudorapidity distribution of charged particles produced in INEL p-$\bar{p}$ collisions at $\sqrt{s} = 630$ GeV. The symbols and curve represent the same meanings as those in Fig. 2, but the experimental data with the statistical errors are taken from the P238 Collaboration [10].

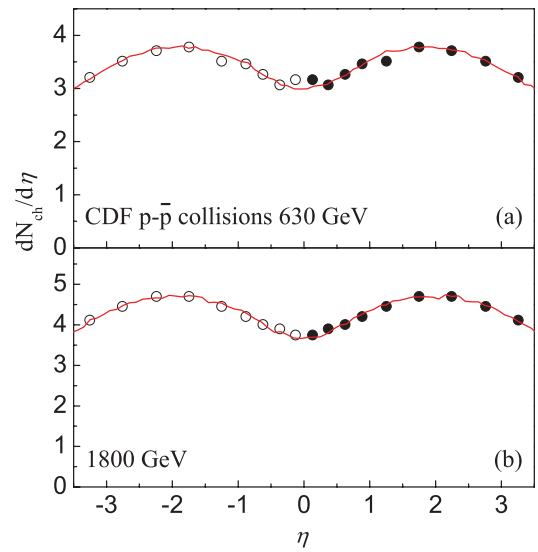

FIG. 5. (Color online) The pseudorapidity distributions of charged particles produced in INEL p-$\bar{p}$ collisions at $\sqrt{s} = 630$ and 1800 GeV. The symbols and curve represent the same meanings as those in Fig. 2, but the experimental data with the statistical errors are taken from the CDF Collaboration [11].

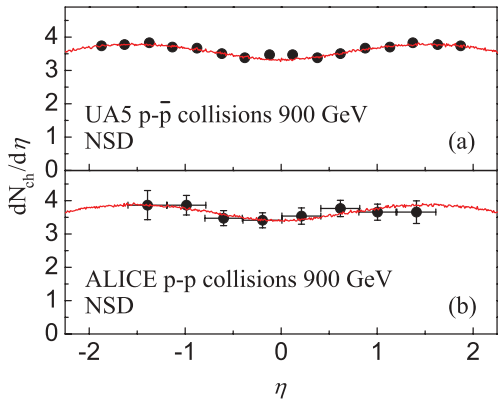

FIG. 6. (Color online) The pseudorapidity distributions of charged particles in NSD p-$\bar{p}$ or p-p collisions at $\sqrt{s} = 900$ GeV. The symbols and curve represent the same meanings as those in Fig. 2, but the experimental data with the statistical errors are taken, respectively, from the UA5 and ALICE collaborations [12].

describes the pseudorapidity distribution of charged particles produced in p-$\bar{p}$ or p-p NSD process at $\sqrt{s} = 900$ GeV.

From the above parameter values, we obtain the dependences of these parameters on $\ln\sqrt{s}$ in Fig. 7. Different symbols represent the results of different collaborations as marked in the figure. The parameter values obtained in Fig. 6 are not included in Fig. 7 owing to the narrow pseudorapidity distribution and unavailable contribution of leading particles. The solid lines denote the linear relationships between these parameters and $\ln\sqrt{s}$ and can be expressed as $y_{P\max} = -y_{T\min} = (0.326 \pm 0.023)\ln\sqrt{s} + (1.415 \pm 0.144)$, $y_{P\min} = -y_{T\max} = (0.033 \pm 0.003)\ln\sqrt{s} - (0.055 \pm 0.016)$, $y_P = -y_T = (0.086 \pm 0.094)\ln\sqrt{s} + (3.650 \pm 0.583)$, $K_P = K_T = -(0.001 \pm 0.001)\ln\sqrt{s} + (0.418 \pm 0.006)$, $k_P = k_T = (0.001 \pm 0.001)\ln\sqrt{s} + (0.082 \pm 0.006)$, and $N_c = (8.496 \pm 0.273)\ln\sqrt{s} - (27.046 \pm 1.696)$. The corresponding

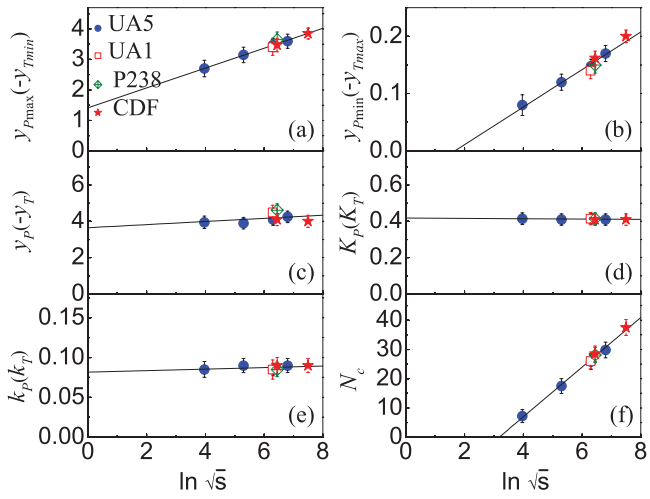

FIG. 7. (Color online) The relationships between different parameters and $\ln\sqrt{s}$. Different symbols represent different parameter values obtained from different experimental collaborations. The solid lines denote the linear relationships between the considered parameters and $\ln\sqrt{s}$.

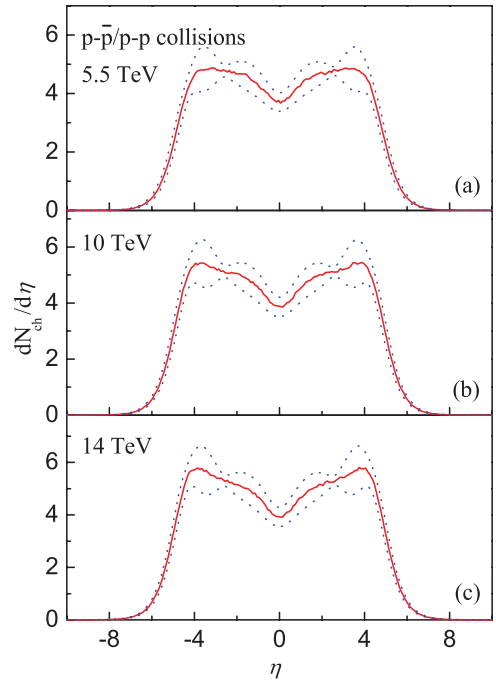

FIG. 8. (Color online) The predicted pseudorapidity distributions of charged particles in INEL p-$\bar{p}$ or p-p collisions at the LHC energies (5.5, 10, and 14 TeV). The solid curves denote the calculated results with the multisource ideal gas model and the dotted curves denote the error ranges obtained by considering the error propagation of all the parameters.

values of χ^2/dof are 0.016, 0.096, 0.327, 0.009, 0.042, and 0.037, respectively.

We could calculate the different parameter values in p-$\bar{p}$ or p-p collisions with the laws above when the energy rises up to 5.5, 10, and 14 TeV at the LHC. The results are expressed as $y_{P\max} = -y_{T\min} = 4.219$, 4.414, and 4.523; $y_{P\min} = -y_{T\max} = 0.228$, 0.247, and 0.258; $y_P = -y_T = 4.391$, 4.442, and 4.471; $K_P = K_T = 0.413$, 0.413, and 0.413; and $k_P = k_T = 0.087$, 0.087, and 0.087. The normalization coefficients N_c are 46.130, 51.209, and 54.068, respectively. The predicted pseudorapidity distributions of the charged particles at the LHC energies are shown in Fig. 8. The solid curves denote the calculated results of the multisource ideal gas model. The dotted curves denote the error ranges of the calculated results. In the calculation of the error ranges, we use the error propagation law described in a textbook on the probability and statistic in experimental physics [42]. All the parameter errors are considered in the propagation.

We point out that the χ^2/dof for an accurate physics model should on average be close to one. The present values in most cases are systematically smaller. This usually implies that the errors on the data are too large or that the system is overdetermined. In our opinion, the real situation is that large relative errors are used in the present work. In fact, the errors are taken to be half the size of the symbols in cases where the error bars are smaller than half the size. Thus, a smaller χ^2/dof can be obtained. The main free parameters in the present work include three rapidity shifts (such as $y_{P\min}$, $y_{P\max}$, and y_P)

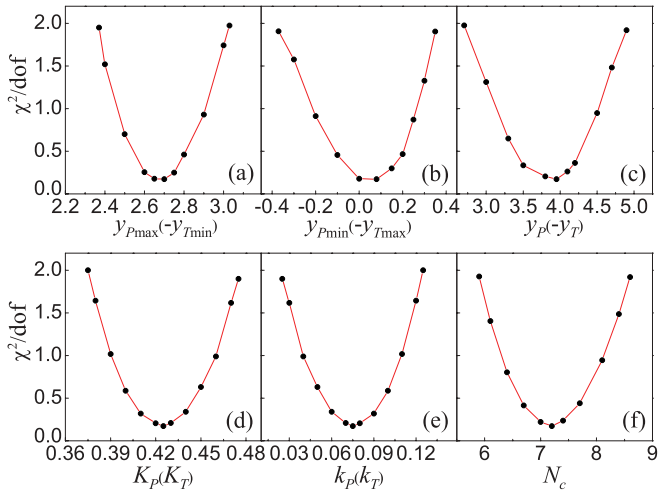

FIG. 9. (Color online) The variation trends of χ^2/dof on different parameters by refitting the experimental data presented in Fig. 2(a). The symbols represent the taken parameter values and the corresponding χ^2/dof values. The solid curves are to guide the eye.

and one contribution (such as K_P or k_P) of the cylinders and leading particles. All of them are very sensitive to the data.

To show how the χ^2 distribution varies with the fit parameters, in Fig. 9 we give the variation trends of χ^2/dof on different parameters by refitting the experimental data presented in Fig. 2(a). In the refitting process, we take more than 10 values for one parameter and let others be the most acceptable values. The symbols in Fig. 9 represent the taken values of the concerned parameter and the corresponding values of χ^2/dof. The solid curves are to guide the eye. We see that the fit is sensitive to the data and the parameters. When we do the fit, as given in Ref. [9], only the statistical errors in the data are quoted.

IV. CONCLUSIONS

With the multisource ideal gas model we have studied the pseudorapidity distributions of charged particles produced in p-$\bar{p}$ or p-p collisions at different energies and compared the calculated results with the experimental data of five collaborations. From the comparison we see that the calculated results are in agreement with the experimental data. From the variation tendency of these parameters we know that the length and distance of the two cylinders in rapidity space increase with the increase of collision energy, and the contributions of the leading particles and other parts to the pseudorapidity distribution are invariable probabilities. We draw the conclusion that the rapidity shifts of the two cylinders are linearly related to $\ln\sqrt{s}$. Moreover, we predict the results of collisions at the LHC when the energy increases to 5.5, 10, and 14 TeV, which will be tested in the near future. We have got sufficient reasons to believe that the multisource ideal gas model is eligible.

ACKNOWLEDGMENTS

This work was supported by the National Natural Science Foundation of China under Grants No. 10975095 and No. 11005003, the Open Research Subject of the CAS Large-Scale Scientific Facility Grant No. 2060205, the Shanxi Provincial Natural Science Foundation under Grant No. 2007011005, and the Shanxi Scholarship Council of China.

[1] B. Alessandro *et al.* (ALICE Collaboration), J. Phys. G **32**, 1295 (2006).
[2] D. G. d'Enterria *et al.* (CMS Collaboration), J. Phys. G **34**, 2307 (2007).
[3] A. Augusto Alves *et al.* (LHCb Collaboration), J. Instrum. **3**, S08005 (2008).
[4] P. W. Higgs, Phys. Rev. Lett. **12**, 132 (1964).
[5] P. Huang, N. Kersting, and H. H. Yang, Phys. Rev. D **77**, 075011 (2008).
[6] L. Maiani, G. Parisi, and R. Petronzio, Nucl. Phys. B **136**, 115 (1979).
[7] S. N. Ganguli and P. K. Malhotra, Phys. Lett. B **42**, 83 (1972).
[8] G. Arnison *et al.* (UA1 Collaboration), Phys. Lett. B **123**, 108 (1983).
[9] G. J. Alner *et al.* (UA5 Collaboration), Phys. Rep. **154**, 247 (1987).
[10] R. Harr *et al.*, Phys. Lett. B **401**, 176 (1997).
[11] F. Abe *et al.* (CDF Collaboration), Phys. Rev. D **41**, 2330 (1990).
[12] K. Aamodt *et al.* (The ALICE Collaboration), Eur. Phys. J. C **65**, 111 (2010).
[13] J. X. Sun, F. H. Liu, and E. Q. Wang, Chin. Phys. Lett. **27**, 032503 (2010).
[14] F. H. Liu, N. N. Abd Allah, D. H. Zhang, and M. Y. Duan, Int. J. Mod. Phys. E **12**, 713 (2003).
[15] F. H. Liu, N. N. Abd Allah, and B. K. Singh, Phys. Rev. C **69**, 057601 (2004).
[16] F. H. Liu and J. S. Li, Phys. Rev. C **78**, 044602 (2008).
[17] F. H. Liu, Nucl. Phys. A **810**, 159 (2008).
[18] X. N. Wang and M. Gyulassy, Phys. Rev. Lett. **86**, 3496 (2001).
[19] A. Capella and D. Sousa, Phys. Lett. B **511**, 185 (2001).
[20] K. J. Eskola, K. Kajantie, P. V. Ruuskanen, and K. Tuominen, Nucl. Phys. B **570**, 379 (2000).
[21] S. Jeon and J. Kapusta, Phys. Rev. C **56**, 468 (1997).
[22] J. Gosset, H. H. Gutbrod, W. G. Meyer, A. M. Poskanzer, A. Sandoval, R. Stock, and G. D. Westfall, Phys. Rev. C **16**, 629 (1977).
[23] G. D. Westfall, J. Gosset, P. J. Johansen, A. M. Poskanzer, W. G. Meyer, H. H. Gutbrod, A. Sandoval, and R. Stock, Phys. Rev. Lett. **37**, 1202 (1976).
[24] J. Aichelin, A. Rosenhauer, G. Peilert, H. Stoecker, and W. Greiner, Phys. Rev. Lett. **58**, 1926 (1987).
[25] U. Eichmann, J. Reinhardt, and W. Greiner, Phys. Rev. C **61**, 064901 (2000).
[26] D. T. Khoa, N. Ohtsuka, M. A. Matin, A. Faessler, S. W. Huang, E. Lehmann, and R. K. Puri, Nucl. Phys. A **548**, 102 (1992).

[27] A. D. Sood and R. K. Puri, Phys. Rev. C **73**, 067602 (2006).
[28] H. Masui, B. Mohanty, and N. Xu, Phys. Lett. B **679**, 440 (2009).
[29] L. Grandchamp and R. Rapp, Phys. Lett. B **523**, 60 (2001).
[30] L. Grandchamp and R. Rapp, Nucl. Phys. A **709**, 415 (2002).
[31] J. P. Blaizot, M. Dinh, and J. Y. Ollitrault, Phys. Rev. Lett. **85**, 4012 (2000).
[32] A. K. Chaudhuri, J. Phys. G **35**, 065105 (2008).
[33] H. Weber, E. L. Bratkovskaya, W. Cassing, and H. Stocker, Phys. Rev. C **67**, 014904 (2003).
[34] W. Cassing, E. L. Bratkovskaya, and A. Sibirtsev, Nucl. Phys. A **691**, 753 (2001).
[35] V. P. Konchakovski, M. I. Gorenstein, and E. L. Bratkovskaya, Phys. Rev. C **76**, 031901 (2007).
[36] S. Eremin and S. Voloshin, Phys. Rev. C **67**, 064905 (2003).
[37] F. H. Liu, Phys. Rev. D **63**, 032001 (2001).
[38] F. H. Liu, Phys. Rev. C **69**, 067901 (2004).
[39] F. H. Liu, Phys. Rev. C **78**, 014902 (2008).
[40] F. H. Liu, Phys. Lett. B **583**, 68 (2004).
[41] F. H. Liu and J. S. Li, Acta Phys. Pol. B **40**, 331 (2009).
[42] Y. S. Zhu, *Probability and Statistic in Experimental Physics*, 2nd ed. (Scientific Press, Beijing, China, 2006), p. 67.